PERGAMON

Deep-Sea Research II 50 (2003) 2049–2075

DEEP-SEA RESEARCH
PART II

www.elsevier.com/locate/dsr2

Variability of water properties, heat and salt fluxes in the Arabian Sea, between the onset and wane of the 1995 southwest monsoon

Lisa M. Beal[a,*], Teresa K. Chereskin[a], Harry L. Bryden[b], Amy Ffield[c]

[a] *SIO-UCSD, 9500 Gilman Drive, La Jolla, CA 92093-0230, USA*
[b] *Southampton Oceanography Centre, Empress Dock, Southampton SO14 3ZH, UK*
[c] *Lamont-Doherty Earth Observatory, Palisades, NY 10964, USA*

Abstract

We investigate the variability of the circulation, water masses, heat and salt fluxes in the Arabian Sea over the course of the southwest monsoon. Two zonal sections taken along 8°30′N in 1995 as part of the Indian Ocean WOCE hydrographic program are used. The first was occupied in early June at the onset of the southwest monsoon winds, the second in late September, at the wane of the monsoon. The September section was found to be generally warmer (+0.32°C) and saltier (+0.04) than in June, despite a 50 mm drop in mean sea level. Therefore, the common assumption that an increase in sea-surface height follows an increase in heat content (the hydrostatic response) does not hold. Instead, we conclude that the heat content increases due to the advection of Arabian Sea Surface Water and Red Sea Water onto the section from the north, and the drop in sea level is due to a loss of mass, rather than heat, from the water column. There are large uncertainties involved in diagnosing the heat-flux divergence across the Arabian Sea, because the seasonal variability of the water masses and circulation in the basin mean that our data are not representative of a steady state. We treat each section separately and find an oceanic heat export of −0.72 PW in June and −0.19 PW in September, implying a basin cooling rate of about −0.36 PW in June and a slight heating of 0.12 PW in September. In June the mass and heat balances are dominated by the Ekman transport and the Somali Current, with very flat density surfaces resulting in a small interior geostrophic transport. By September the Ekman transport has reduced, and it is primarily the interior transport that balances a strong Somali Current. There are two main overturning cells in June and September: A shallow one of approximate magnitude 15 Sv in June and 0 Sv in September, which reaches depths of no more than 500 m and is driven by Ekman divergence at the surface; and a deep cell of magnitude 1 Sv representing a weak inflow and subsequent upwelling of Circumpolar Deep water. The deep cell implies a basin-averaged upwelling velocity of 3.2×10^{-5} cm s^{-1} through 2200 m.
© 2003 Elsevier Science Ltd. All rights reserved.

1. Introduction

As a component of the WOCE and the NOAA-repeat hydrographic programs in the Indian Ocean, two zonal sections were occupied in the Arabian Sea during the onset (June) and wane (September) of the 1995 southwest monsoon. Each

*Corresponding author. Rosenstiel School of Marine and Atmospheric Science, University of Miami, 4600 Rickenbacker Causeway, Miami, FL 33149-1098, USA. Tel.: +1-305-361-4093; fax: +1-305-361-4696.
E-mail address: lbeal@rsmas.miami.edu (L.M. Beal).

0967-0645/03/$ - see front matter © 2003 Elsevier Science Ltd. All rights reserved.
doi:10.1016/S0967-0645(03)00045-6

section crossed from Somalia to Sri Lanka nominally along 8°30′N, enclosing the Arabian Sea to the north. These data provide a unique opportunity to diagnose the absolute circulation of the Arabian Sea and thus its heat and freshwater fluxes at different stages of the monsoon cycle using an inverse model.

The oceanic heat budget of the Arabian Sea during the southwest monsoon is a complex balance of atmospheric forcing, large interior Ekman transports, vigorous coastal upwelling, an inflow of equatorial waters along the western boundary, and a potential change in ocean heat content (or storage). Estimates of the atmospheric component, that is the net air–sea heat flux over the Arabian Sea during the southwest monsoon, have lately swung from small and negative to large and positive. The older climatologies of Oberhuber (1988) and Hastenrath and Lamb (1980) both estimated net oceanic heat loss during the southwest monsoon, of order $-10\,\mathrm{W\,m^{-2}}$. Recently, Weller et al. (1998) published air–sea flux measurements from a surface buoy deployed off the coast of Oman, a region associated with some of the strongest winds of the southwest monsoon. The net heat flux during the 1995 southwest monsoon (1 June–15 September) was $89.5\,\mathrm{W\,m^{-2}}$ at the buoy, and evaporation minus precipitation (E-P) was $0.1603\,\mathrm{mm\,h^{-1}}$. These measurements compare very well with the new SOC climatology (Josey et al., 1996), with differences of just $3\,\mathrm{W\,m^{-2}}$ for the net heat and $0.0086\,\mathrm{mm\,h^{-1}}$ for E-P. While these recent estimates are consistent, there are still large errors associated with the bulk parameterisations used to calculate air–sea fluxes. For instance, the SOC climatology exhibits a global inbalance of $30\,\mathrm{W\,m^{-2}}$ and it is unclear where or how this bias should be accounted for.

The variability of heat content in the Arabian Sea is not dominated by the seasonality of solar irradiance, as it is in other parts of the world ocean, although clearly the air–sea fluxes are large and important. In fact, Düing and Leetmaa (1980) estimated that despite a positive net heat flux from the atmosphere, the Arabian Sea cools significantly during the southwest monsoon and the heat loss is owing to a southward oceanic heat flux across the equator and upwelling of cold waters along the coast of Arabia. Using monthly, gridded XBT data, from the surface-to-400 m depth, Hastenrath and Greischar (1993) also found that the Arabian Sea loses heat over the course of the southwest monsoon. They calculated a loss of order $100\,\mathrm{Wm^{-2}}$ and, combining this with values of net air–sea heat flux from ship observations, deduced an advective ocean heat export of as much as $150\,\mathrm{W\,m^{-2}}$ during the southwest monsoon. Heat storage has also been estimated from sea-surface height (SSH) data, by using the assumption that sea-level change is directly proportional to heat content (Chambers et al., 1997). Using TOPEX/Poseidon altimeter data and model simulations, Manghnani et al. (2002) found that there are two main modes of heat content redistribution in the Indian Ocean: the first is an offshore and southward propagation of heat in the northern Indian Ocean associated with southwest monsoon winds, and the second is associated with equatorial Rossby waves that dynamically readjust the ocean after the monsoon wind forcing is relaxed. Their estimated loss of heat content in the Arabian Sea during the southwest monsoon based on SSH anomalies is also $150\,\mathrm{W\,m^{-2}}$.

There are some limitations in each of these studies that make this problem worth revisiting. Düing and Leetmaa (1980) did not consider a mass-conserving volume, which is essential when closing the heat budget (Bryden et al., 1991). In particular, they did not account for the heat flux of the fast-flowing Somali Current at the western boundary. Hastenrath and Greischar (1993) did not consider mass conservation either. Implicitly their study requires a closure of the mass budget over the top 400 m of the water column, but whether such a closure exists is not discussed. Finally, estimating heat content from SSH anomaly (Manghnani et al., 2002) discounts both the barotropic response of the ocean to wind forcing as well as the effect of variations in salinity on seawater density (Chambers et al., 1997). In the northern Indian Ocean, where variability is dominated by the annual monsoon cycle of winds, it is likely that the barotropic changes in SSH are significant in each season. Moreover, in the Arabian Sea evaporation rates are exceptionally high during the southwest monsoon and resultant

salinity changes are large. We have estimated the effect on SSH of a change in salinity of 0.6, the difference between the mean salinity of the mixed layer in September and in June, and found that up to 50% of the SSH signal could be due to density variations resulting from salinity rather than temperature change.

In this paper, we revisit the heat budget of the Arabian Sea using direct ocean measurements. We conserve mass and calculate separate heat and salt budgets for June (beginning of southwest monsoon), and September (end of southwest monsoon), and highlight the differences in the circulation, transports and water mass structures at these times.

2. Data

The 1995 southwest monsoon was a typical one in strength, although characterized by a double onset (Fieux and Stommel, 1977) in which a small southwesterly wind event from beginning to mid-May was followed by a 2-week lull in the winds (Flatau et al., 2001). The 'real' monsoon began on the 1 June, with constant southwesterly winds (237° on average) blowing until 15 September. The wind speed over the Arabian Sea increased steadily until mid-June, peaked at $15\,\mathrm{m\,s^{-1}}$ in mid-July, then dropped off slightly to a consistent $10\,\mathrm{m\,s^{-1}}$ throughout August and September (Weller et al., 1998).

Eddy-resolving hydrographic measurements were collected on two zonal traverses across the southern Arabian Sea during the 1995 southwest monsoon, as part of the WOCE hydrographic program (WHP) in the Indian Ocean. In early June, just a few days after the onset of the winds, NOAA repeat line IR1 began 20 km off the coast of Somalia, crossing the Arabian Sea along 8°30′N and diverting southward in the east to finish in Sri Lanka (triangles in Fig. 1). At the end of the monsoon in mid-September, WHP line I1 crossed the Arabian Sea again along 8°30′N, with diversions off the zonal track to cross normal to topography at the boundaries and over ridges, finishing off the west coast of India (circles in Fig. 1). The 8°30′N sections cross two

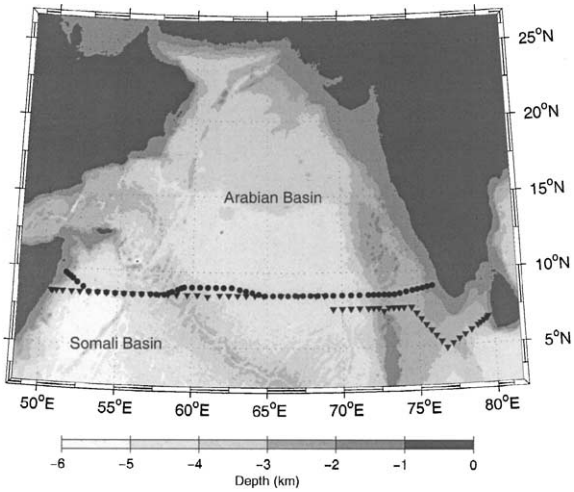

Fig. 1. Map showing the station locations for June (triangles) and September (circles), and the basin bathymetry in grey shading. The Carlsberg Ridge runs northwest–southeast, reaching the equator at about 65°E, and the Chagos-Laccadives Ridge runs north–south at 73°E.

ridge-systems, the Carlsberg Ridge in the west and the Chagos-Laccadives Ridge in the east, and enclose the Arabian Sea and its marginal seas, the Red Sea and the Persian Gulf, to the north. The Carlsberg Ridge cuts off the Arabian Basin from inflowing waters below about 3800 m (Fig. 1), whereas the Somali Basin in the west can fill with denser waters from the south.

Full-depth combined conductivity-temperature-depth-oxygen (CTDO2) and lowered acoustic Doppler current profiler (LADCP) measurements were taken at each station during each cruise. During the September cruise there was LADCP failure on three stations within a strong anticyclonic eddy in the Somali Basin called the Great Whirl (stns 906–908), and at another five stations (stns 934–938) at the centre of the Arabian Basin. In the Great Whirl data loss was restricted to below 1200 m depth, and below this we extrapolated linearly to zero velocity at the seabed. However, the discontinuous shear trace also degrades the absolute ocean velocities obtained above this depth, making errors larger. No attempt was made to fill the 275-km gap in the Arabian Basin. The estimated error for absolute current from LADCP on all other stations is about

$4\,cm\,s^{-1}$ (Beal and Chereskin, 2002). Thirty-six bottle samples were collected on each station during September and 24 during June, at various depths throughout the water column. Nutrients (silicate, nitrate and phosphate) were measured on both cruises; however, due to an analyser failure during the cruise and subsequent degradation of the samples during frozen storage and thawing (Chapman and Mostert, 1990), the data from June were found to be untenable. Salinity and temperature were sampled, processed and calibrated to WOCE standards on the June cruise (WOCE CTD specs for temperature: accuracy 0.002°C and precision 0.0005°C, and for salinity: accuracy 0.002 and precision 0.001). However, instrumental problems during the September line doubled salinity errors (temperature: accuracy 0.002°C and precision 0.001°C, and salinity: accuracy 0.004 and precision 0.002). Bottle salinity and oxygen data from each occupation compare closely (on pressure surfaces) and are therefore suitable for studies of changes in water masses (Fleurant and Molinari, 1998). Continuous shipboard ADCP (SADCP) measurements were collected on station and underway during both cruises. GPS navigation was P-code accuracy, and a four-attenae array measured the ship's attitude. As a result, errors in the ocean current from SADCP are less than $\pm 2\,cm\,s^{-1}$(Chereskin et al., 1997).

3. The inverse model

Each of the two hydrographic sections described above enclose the Arabian Sea to the north, allowing for conservation statements of mass, salt and silicate (the latter used in September only). We implemented a Gauss–Markov inverse (Wunsch, 1996) to impose these constraints on the circulation. Seven neutral density layers (Jackett and McDougall, 1997) were chosen as constraints and for the diagnosis, based on water mass properties (Table 1). Layer one penetrates from the surface to an average 60 m depth and represents Bay of Bengal surface waters. In June this top layer also coincides approximately with the mixed-layer depth. Layer two encompasses Subtropical Surface Waters (STSW) and the salty Arabian Sea Surface Waters (ASSW), which are formed locally during the southwest monsoon. Persian Gulf Water (PGW) influences layer 3 which covers the thermocline from about 150–400 m depth. Layer 4 is a wide density band (26.9–27.6) where signatures of salty Red Sea Water (RSW) are found and also the intermediate oxygen minimum, which originates in the northern Arabian Sea. North Indian Deep Water (NIDW) is characteristic below 1100 m (layer 5) and Circumpolar Deep Water (CDW) below approximately 2200 m with neutral densities over 28.0 (layer 6). Finally, layer 7 encompasses the dense bottom water of the Somali Basin that is prevented from filling the bottom of the adjoining Arabian Basin by the topography of the Carlsberg Ridge.

Table 1
Neutral density layers defining water masses of the Arabian Sea

Layer	Water mass	Neutral density	Approx. depth (m)
1	Bay of Bengal surface water	<23.5	<60
2	Arabian sea surface water	23.5–25.4	60–150
3	Persian Gulf water and thermocline waters	25.4–27.1	150–400
4	Red sea water	27.1–27.6	400–1100
5	North Indian deep water	27.6–28.0	1100–2200
6	Circumpolar deep water	28.0–28.115	2200–3800
7	Somali Basin bottom water	>28.115	>3800

For both June and September mass was conserved in the top two layers combined and then in each layer below, balanced to within ± 1Sv, and from top-to-bottom within 0 ± 0.5 Sv. In the Arabian Sea there is ventilation and formation of new water masses seasonally down to layer 2, layer 3 outcrops in the Arabian Gulf where PGW is formed, and layer 4, containing RSW, is ventilated in the Red Sea. Therefore, salt (salinity anomaly) conservation in the upper four layers (and top-to-bottom) is not enforced, leaving a salt conservation statement in layers 5, 6, and 7 only. In the September case a top-to-bottom silicate conservation was used (Robbins and Toole, 1997); however, nutrient data from June

were not of sufficient quality. We followed Ganachaud et al. (2000) to set the error of the enforced balance for salinity anomaly, which depends on the variance of salinity values and the uncertainty of the mass balance. In the case of silicate we prefer to use the uncertainty estimated from the size of biogeochemical sources and sinks, $\pm 200\,\mathrm{kmol\,s^{-1}}$ (P. Robbins, personal communication).

Dianeutral fluxes of salt were permitted in the inverse model by both advection (w^*) and diffusion (k^*) between layers. Diffusion was used as a constraint by giving it an initial value of $10 \pm 10\,\mathrm{cm^2\,s^{-1}}$, based on micro-structure measurements of the deep ocean (Polzin et al., 1997). Dianeutral velocity was allowed effectively free adjustment across interfaces at the bottom of layers 2 and 3 ($\pm 10 \times 10^{-2}\,\mathrm{cm\,s^{-1}}$), because of expected large Ekman-driven upwelling into the surface layers (Smith and Bottero, 1977), plus outcropping of these layers in the north. For the deep ocean, magnitudes were allowed to adjust within $\pm 5 \times 10^{-5}\,\mathrm{cm\,s^{-1}}$ (Munk and Wunsch, 1998). For the air–sea interface, the Weller et al. (1998) buoy data were used to set an expected scale (in the covariance matrix) for the E-P flux of the Arabian Sea. These are 0.3 Sv in June and 0.15 Sv in September. Interfacial property values and gradients in the Arabian Sea north of 8°30′N, on which w^* and k^* operate, were estimated from the NODC database using data from May through October (summer monsoon). There are large seasonal changes in properties on the top four interfaces, and this will be expanded on later when we discuss the June and September property fields. The areas of the interfaces were estimated from the Smith and Sandwell (1997) bathymetry, by using the area of the mean depth of each neutral surface. The area of the interface at the top of layer 7 is difficult to estimate, since this neutral surface plunges into the seabed within the Somali Basin and does not reappear in the Arabian Basin. Therefore, its area has been taken approximately as one-quarter of the area of its mean depth.

Initial zero-velocity surfaces (ZVS) for the geostrophic shears in the interior of the ocean in both June and September were estimated to lie on the interface between equatorward flowing NIDW and northward flowing CDW, along neutral surface 28.0 (about 2200 m depth). The authors had hoped to utilise direct velocities in the ocean interior to initialise the geostrophic velocity field before executing the inversion. However, we found (as did Bryden et al., 1991) that this approach introduced unrealistically large deep velocities over the abyss as well as strong, alternating north and south flows over the Chagos-Laccadives Ridge and towards the eastern boundary (especially in June). The latter effect occurred despite removing barotropic tides from the LADCP data using a model with assimilated TOPEX data (Egbert et al., 1994). In addition, the initial circulation was pushed farther from mass balance. We concluded that the direct measurements are too noisy in the ocean interior, where small mean currents are obscured by rapidly changing barotropic flows. We maintained use of the direct velocities for initialising the velocity field within the Somali Basin, however, where the Somali Current and the Great Whirl are large signals.

Direct velocities from LADCP were used to estimate the ZVS at the western boundary, where barotropic currents were a maximum of $45\,\mathrm{cm\,s^{-1}}$ in the Somali Current in September. A careful analysis of the western boundary current (WBC) was made for both June and September and is described in Beal and Chereskin (2002). Its size is of critical importance in quantifying the circulation (Bryden and Beal, 2000). As a result, a mass constraint of 37 ± 5 Sv for the volume transport of the Somali Current (including 14.6 Sv of off-section transport) and an additional -10 ± 5 Sv for the net transport across the Great Whirl over the upper 1200 m (layers 1–4) were added to the September inverse calculation. Quantifying the western boundary fluxes in June was problematic because no WBC was observed in the hydrographic data, despite evidence from AVHRR sea-surface temperature images, suggesting that generally a cold boundary current existed in June. Thus, we impose only a loosely constrained equation for the net transport across the (underdeveloped) Great Whirl, 6 ± 5 Sv, which was observed at the western boundary. For a detailed description of the velocity structures and

transports at the western boundary in both June and September see Beal and Chereskin (2002). Finally, a deep WBC was observed in direct velocities in June (Beal et al., 2000a, b), with most of the bottom-intensified current occurring within the bottom triangle gaps that result from the geostrophic calculation. The bottom triangle transport of the DWBC was 3 Sv below 3800 m (sill depth), which must recirculate in the Somali Basin, and this was accounted for in the layer 7 mass balance equation for June.

The Ekman transports for each circulation (June and September) were estimated in Chereskin et al. (2002), using the ageostrophic component of the shipboard ADCP velocities. The Ekman layer depth, as estimated by tracing the top of the pycnocline in June and September, varied profoundly in both time and space and was an important factor for accurately estimating the Ekman transports. In June the top of the pycnocline was equivalent to mixed-layer depth, the estimator most commonly used to set Ekman layer depth, but in September it was much deeper and this had a significant effect on estimated Ekman heat and salt fluxes. Thus, we have retained the vertical and horizontal structure of the Ekman transport (see Chereskin et al., 2002) for our diagnosis of the circulation here, rather than simplifying the Ekman layer as a slab of constant depth and velocity. In June the volume transport is contained within density layer 1 (<60 m depth) and is a huge -19.7 Sv. In September the Ekman layer has deepened and most of the -7.3 Sv transport is within layer 2. Both these direct estimates fall within 1 Sv of indirect estimates from in situ wind data.

4. Results

4.1. Water mass changes during the course of the southwest monsoon

Significant temporal changes in water mass characteristics along 8°30′N were expected within the Ekman and ventilated layers of the Arabian Sea, resulting from a combination of monsoonal water mass formation and strong southeastward Ekman transports between June and September. In fact, what we observe is significant water mass changes as deep as 1300 m.

By September the temperature of the mixed layer at 8°30′N is cooler than it was in June, particularly in the west where the difference is more than 2°C (Fig. 2a). This is despite a net heating through the surface during the southwest monsoon of about 89.5 W m^{-2} (Weller et al., 1998). In addition, the mixed-layer depth is unchanged at about 25 m in both June and September (Chereskin et al., 2002), despite strong winds causing mechanical mixing and densification by evaporation. Assuming these results to be applicable to the Arabian Sea in general, a time series of air–sea fluxes collected at a buoy array at 15.5°N and 61.5°E show why they may not be as counterintuitive as they first appear. Weller et al. (1998) find that wind speed and therefore latent heat loss is high throughout June and July, reducing the net heat flux to near zero, but in the latter half of the monsoon, during August and September, the winds weaken; accordingly the latent heat loss is much reduced and the net heat flux peaks at 200 W m^{-2}. Therefore, peak mixed-layer depths likely occurred in late July (climatologies show peak MLD in August) and shoaled again into September. As for surface temperatures, the effect of evaporative cooling dominates the seasonal summer heating during the first half of the monsoon, to produce lowest SST's in August (Weller et al., 1998). In the remaining month or so of very high net heat flux at the end of the monsoon the mixed layer is thickest (to start with), distributing the heat over more volume and thus failing to return Ekman layer temperatures to their June values. The lowest near-surface temperatures on the September section are in the west where the winds are most intense, but also where the Somali Current and Great Whirl have advected cooler waters from the south.

The mixed layer is salinified and oxygenated throughout the monsoon to form ASSW, in response to solar- and wind-driven high evaporation rates and mechanical mixing (Figs. 2b and c). Southward advection within the Ekman layer also plays a role in the appearance of these waters at 8°30′N. ASSW dominates the surface layer

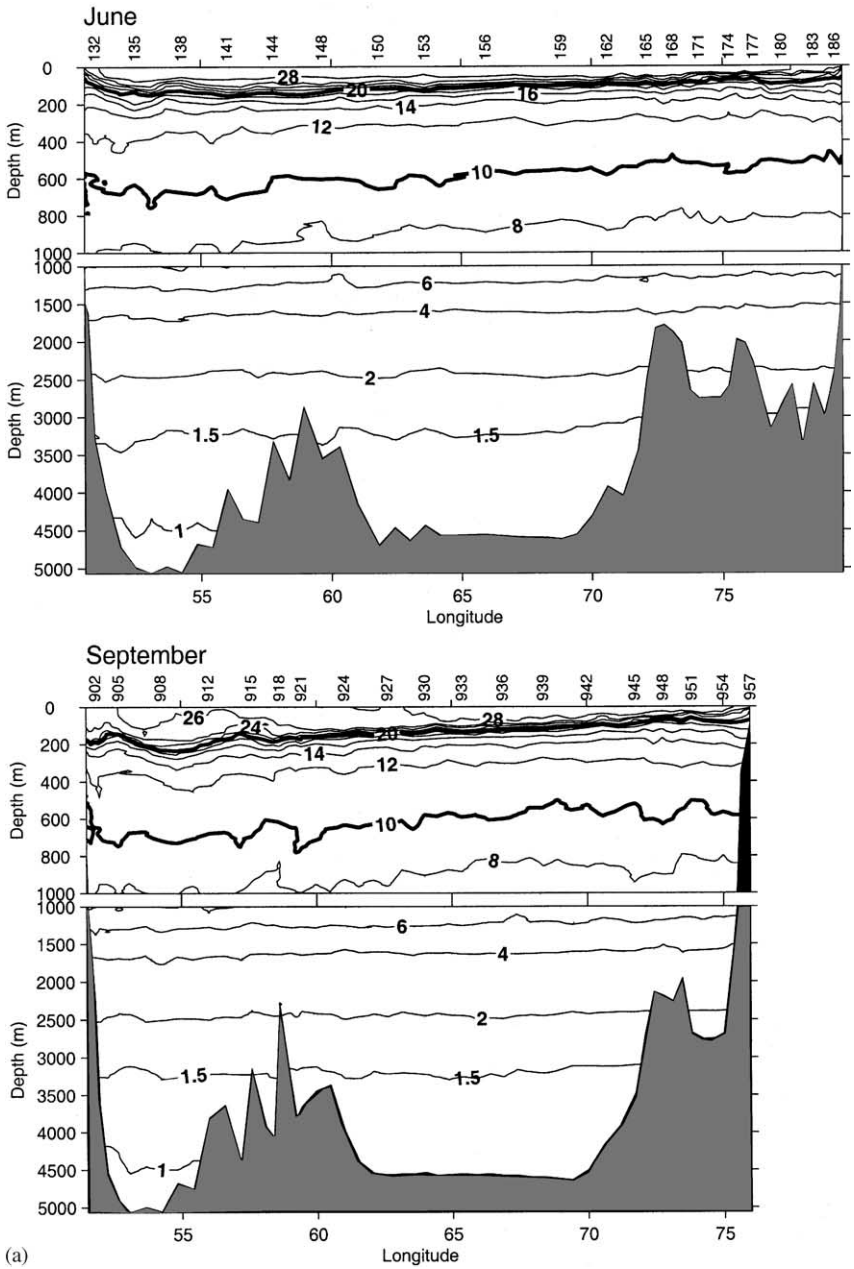

Fig. 2. (a) Vertical sections of potential temperature from Somalia (left) to Sri Lanka/India (right) along 8°30′N in (top panel) June, and (bottom panel) September. Depth is split at 1000 m, with an expanded top panel to show thermocline and surface waters more clearly. Isotherms are in °C, with 10°C and 20°C isotherms shown as thick lines. Every third station number is labelled along the top axis. (b) As (a), but for salinity. Shading changes for every 0.1 salinity change. Thick lines depict neutral density interfaces between water mass layers (at $\gamma = 23.5$, 25.4, 27.1, 27.6, 28.0, and 28.115. See Table 1). (c) As (b), but for oxygen, in $\mathrm{ml\,l^{-1}}$. Shading changes for every $0.25\,\mathrm{ml\,l^{-1}}$ of oxygen.

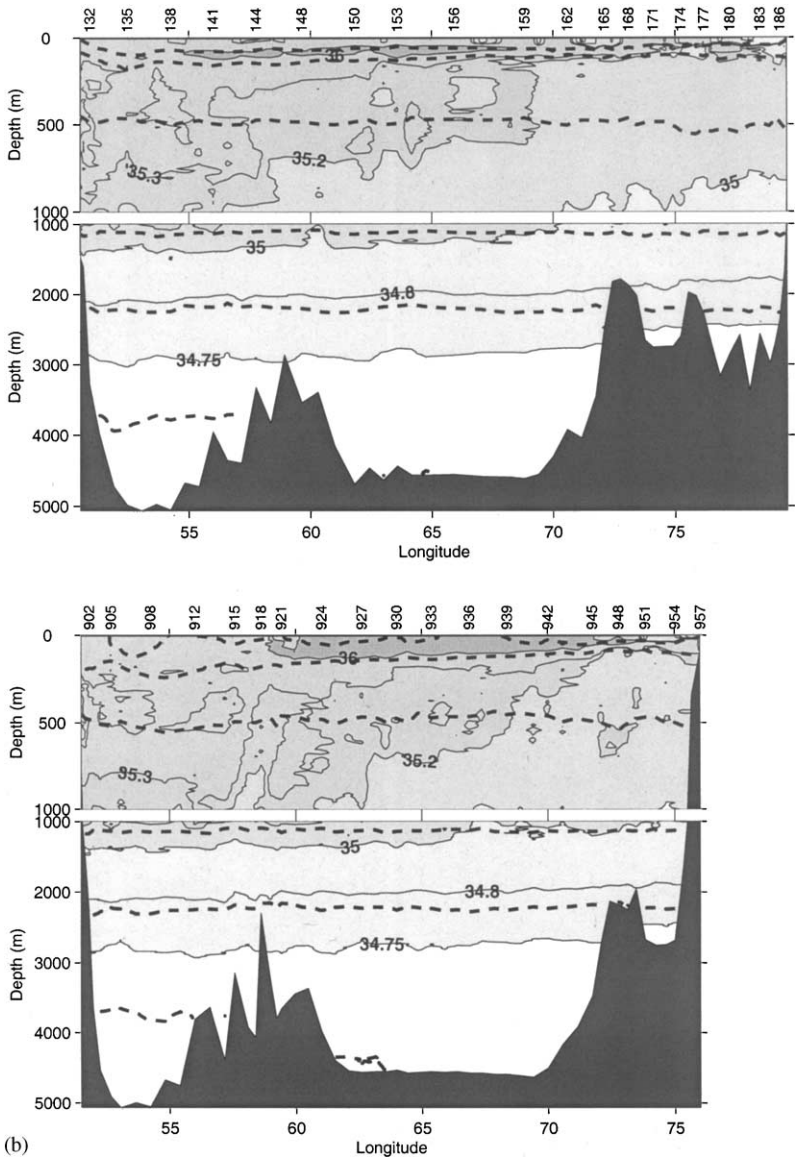

Fig. 2 (*continued*).

everywhere in the ocean interior in September. However, in the west, within the Somali Current and Great Whirl, waters are fresher and cooler than in June, indicating a southerly origin. In the east, fresh Bay of Bengal waters are evident in June, but reduced in September, when we deduce that southward advection has brought saltier and lower oxygen waters from inside the Arabian Sea onto the section. Indeed there is evidence for a net advection of more northerly waters onto the section all the way down to mid-depths. More salty water, attributed to PGW, is present within the thermocline by the end of the monsoon, and there are also large salinity changes within the RSW density layer (Fig. 2b), which will be discussed in more detail below.

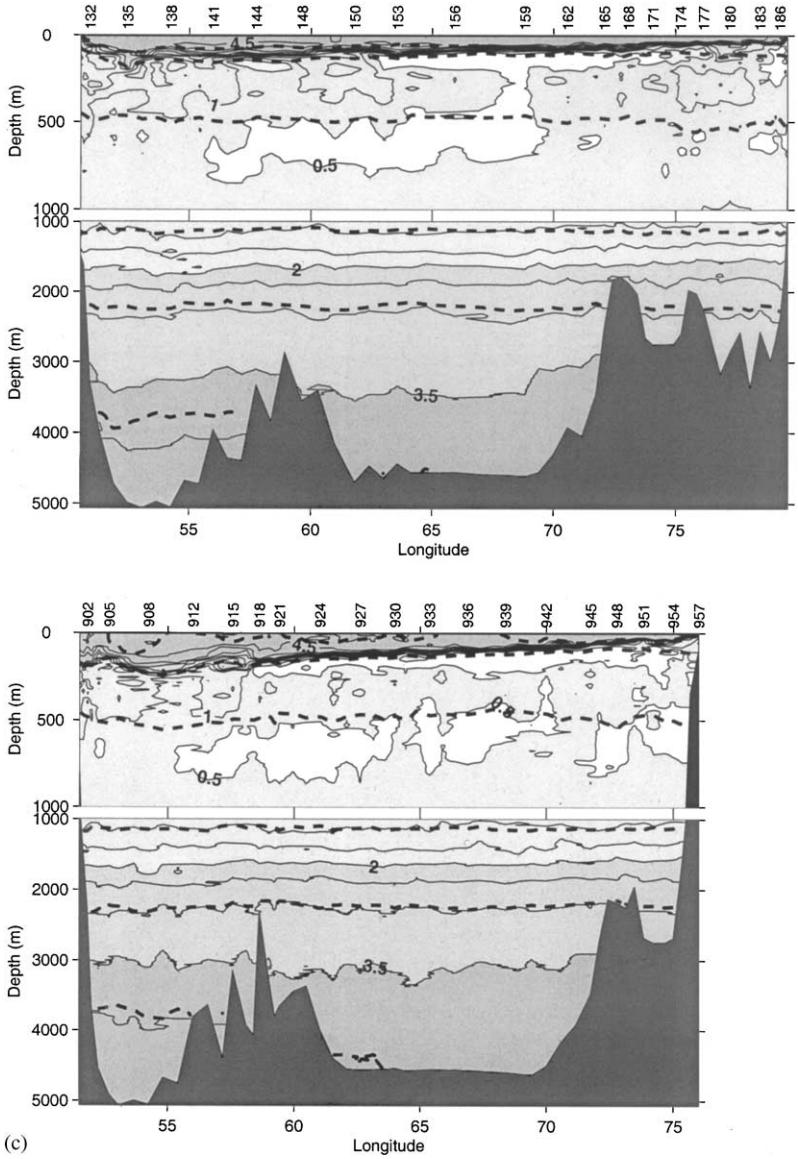

Fig. 2 (*continued*).

The top of the pycnocline (TTP) deepens between June and September, from 46 to 115 m on average (Chereskin et al., 2002). Most of this deepening is in the west, where TTP depth reaches 300 m at 55°E, and results from the downward distortion of density surfaces by the Great Whirl (Fig. 2a). The bottom of the pycno(thermo)cline does not deepen, but remains at 417 m, as demarked by the 12°C isotherm (roughly the bottom of our layer 3). This indicates that there may be an upwelling of water from the shrinking thermocline to the surface through the TTP. In fact, climatological data (Levitus et al., 1994) show that the thermocline thins throughout the region (and not just at 8°30′N), supporting the likelihood of large upwelling. Many investigators have

reported strong coastal upwelling in the western Arabian Sea during the southwest monsoon (Shi et al., 2000; Fischer et al., 2002; Smith and Bottero, 1977), and upwelling transports have been estimated to be around 0.5 Sv to as much as 8 Sv off the coast of Oman. When we discuss the circulation in the following section, the transports within these upper layers are quantified and the balance between advection, upwelling, and storage is discussed further.

The T/S curves for June and September (Fig. 3) illustrate appreciable changes in mean water mass properties along neutral density surfaces, down to waters of 5°C. This is well within the NIDW layer (Figs. 2a and c). Except in the surface layers, where ventilation has changed water mass properties, these changes must be effected by advection. In September the waters are on average warmer and saltier than in June and thus have been advected from the north, deeper inside the Arabian Sea. One could hypothesise that the water column is adjusting barotropically to the monsoon winds. In other words, that a change in Ekman transport plus the WBC transport at any time could be matched by a shift in the barotropic component of the interior transport field, whilst the interior baroclinic transport profile remains the same. Indeed, on short time scales this must be the case, for there is no time for a baroclinic response to the winds. However, our sections are 3.5 months separated, allowing sufficient time for a significant baroclinic change. In fact, SSHA images show that annually forced, baroclinic Rossby waves (propagating intramonsoonally from the west coast of India) are a dominant adjustment mechanism for the circulation in the Arabian Sea (see Discussion).

In any case, we can test this hypothesis approximately by looking at the differences in

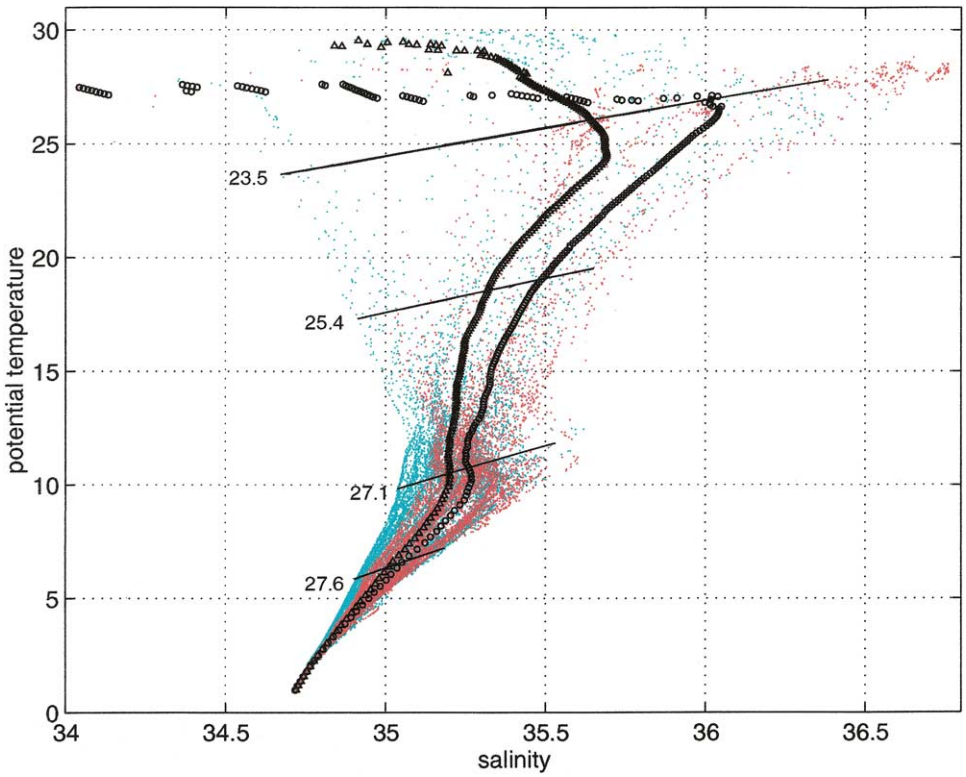

Fig. 3. Potential temperature–salinity scatter diagram for June (blue), and September (red). Black symbols show the mean water mass curves for June (triangles) and September (circles), averaged along neutral density surfaces. Contours of neutral density are shown for water mass interfaces down to the top of the deep waters (see Table 1).

potential temperature and salinity on neutral surfaces between June and September. If a barotropic flow alone is responsible for the advection of more northerly waters onto 8°30′N, then we may expect that the normalised T/S differences (property differences averaged along a neutral surface and normalised by the meridional variance of T/S on that neutral surface) be the same for all depths (densities). These differences are shown in Fig. 4. The meridional, epineutral property variances are determined using data from WOCE line I7, which runs approximately north–south between 8 and 15°N at 64.5°E. Evidently the normalised difference is not the same for all densities, but has a clear maximum at $\gamma = 25.2$, suggesting maximum southward advection of ASSW and PGW. However, noise is considerable, especially in the deep water, where differences and variances tend to zero. In summary, the evidence from water mass properties, although inconclusive, is towards significant baroclinic change across 8°30′N. It is clear that substantial changes in T/S are not limited to the surface layer of the ocean, but rather penetrate to the bottom of the RSW layer at about 1500 m ($\gamma = 27.6$).

Fig. 5 shows sections of potential temperature and salinity changes that occurred between the June and September occupations. Property differences were calculated by pairing those June and September stations closest in longitude, regridding the T/S data onto neutral surfaces (Jackett and McDougall, 1997), and then subtracted June values from those in September. Hence, they illustrate water mass changes along a neutral surface and not water mass changes resulting from isopycnic heave. Stations east of 7°E were not used because here the cruise tracks diverge (Fig. 1). The vertical axes of the sections in Fig. 5 represent only

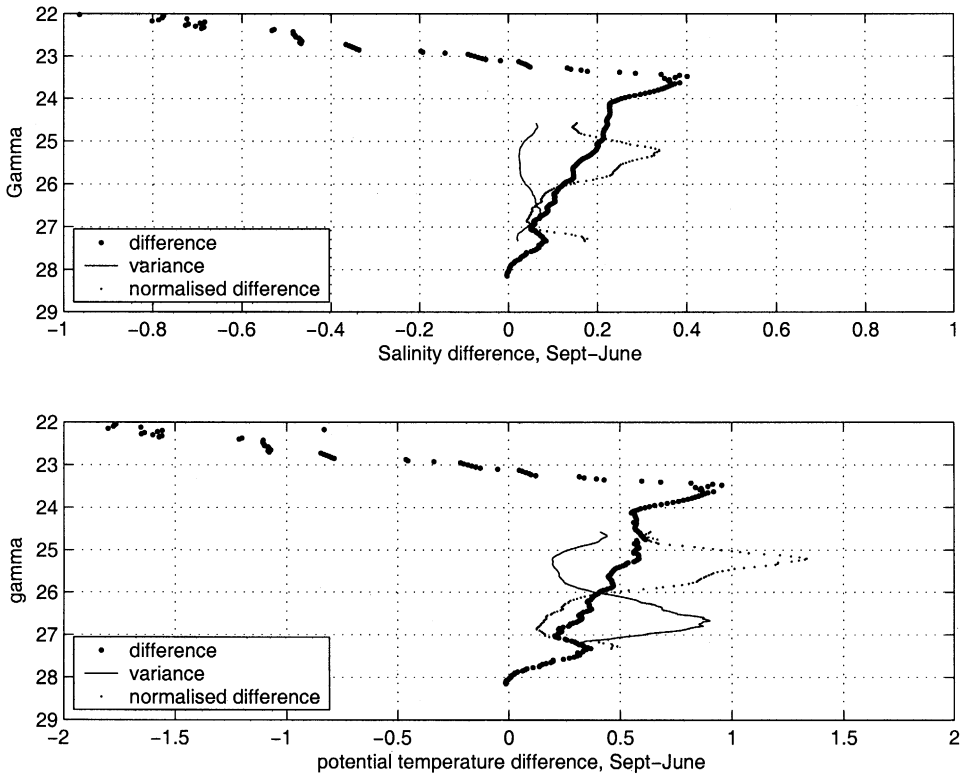

Fig. 4. September–June property differences calculated along neutral surfaces (γ). The top panel shows salinity difference, the bottom panel shows temperature difference (°C). Property differences have been normalised with meridional epineutral variance, calculated from the WOCE I7 data.

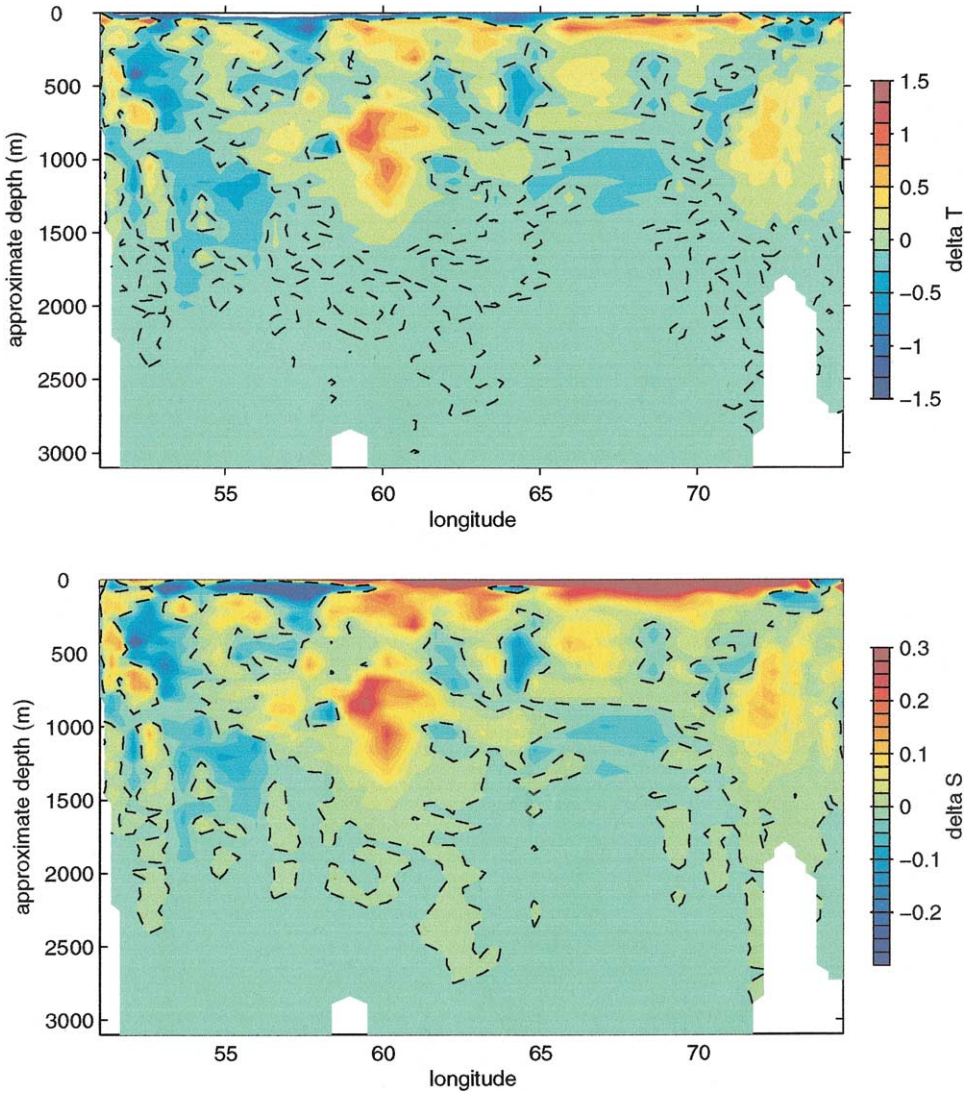

Fig. 5. Vertical sections of (a) potential temperature (°C), and (b) salinity differences along neutral surfaces (September–June). Depth scale is approximate since neutral surfaces are not flat. The black dashed line depicts the zero anomaly contour.

an approximate depth, since the neutral surfaces are not flat and may have moved up or down between occupations. The distribution of property changes along the 8°30′N section is not smooth (Figs. 5a and b), particularly at intermediate depths. Patches of RSW appear above the eastern flank of the Carlsberg Ridge and the western flank of the Chagos-Laccadives Ridge in September, as depicted by higher salinities (+0.2) and temperatures (+1.5°C) centred at 900 m depth. In both June and September, RSW is also present near the western boundary in the Somali Basin (Fig. 2). This supports previous evidence that there may be an export of RSW through the interior of the Arabian Sea during the southwest monsoon, whilst during the northeast monsoon RSW is exported predominantly along the western boundary (Gamsakhurdiya et al., 1991; Beal et al., 2000a, b). At the surface, the Somali Current and Great Whirl have brought cooler surface

(super-thermocline) waters to 8°30′N in the west. In contrast, to the east of the Carlsberg Ridge there is a pool of warm and salty ASSW (discussed above) that has formed during the southwest monsoon.

4.2. The circulation

4.2.1. Challenges

A number of novel challenges were faced in setting up inverse models to quantify the circulation of the Arabian Sea. Foremost is that it is impossible to treat the circulation as representative of a long-term mean, since it switches rotation entirely twice per year during each intermonsoon period. In addition, the flows at the western boundary, the Somali Current and Great Whirl, are non-steady. Movies of sea-surface height anomaly (SSHA) from TOPEX/Poseidon show that the Great Whirl is fast varying and can shift in position by a few degrees within 10 days. Model simulations (M. Luther, personal communication) and observations (Swallow and Bruce, 1966) suggest that the intensity of the Somali Current also fluctuates rapidly in response to the fluctuating wind field, as well as more slowly in response to the annual monsoon forcing.

Despite the varying circulation, changes in SSHA show that top-to-bottom mass conservation is valid at any point in time. Over the course of the southwest monsoon in 1995, between the June and September occupations at 8°30′N, TOPEX Poseidon indicates a gradual drop in SSHA of 71 mm throughout the Arabian Sea. Should this reduction in sea level be attributed solely to a loss (divergence) of mass from the basin (ignoring possible loss of heat), it nevertheless represents a transport of less than 0.05 Sv. Therefore, mass may be tightly conserved and storage is insignificant. However, this assumes an instantaneous data set, when in fact the sections are non-synoptic, each taking 14 days to complete. We cannot make a quantitative test, but animations of SSHA show that mesoscale variability at least, is significant on these time scales. In addition, storage effects may still be important when considering mass conservation in individual layers. As we saw in the temperature and salinity sections (Fig. 2), upper-ocean layer thicknesses change dramatically between occupations at 8°30′N. We used monthly climatological data from the Arabian Sea north of 8°30′N (Levitus et al., 1994; Levitus and Boyer, 1994) to find that layer 3 (the pycnocline) thins by 10 ± 2 m through June (with the error derived from the difference between a linear and spline fit to the trend), reaching its thinnest in August, and thickening again towards September. These numbers are uncertain due to the sparcity and spatial incoherence of the monthly data; however, such a thinning accounts for a loss of approximately 10 Sv from layer 3. Meanwhile, layer 2 thickens by about the same amount, causing a compensatory effect, so that over the top three layers combined, storage is small. In the deeper layers storage is negligible.

The effect of this temporal change in layer thickness on the inverse calculation is this: It changes the interpretation that any mass divergence/convergence in the surface layers results in downwelling/upwelling through their interfaces. Instead, the result may be a change in layer thickness. It does not change the fluxes at 8°30′N. We will discuss this quantitatively in the Overturning section. A much greater problem for our inverse calculation is the temporal variability of the currents. For the June section, which was taken at the onset of the monsoon when the circulation is still spinning up, variability is a problem. Errors from our inverse calculation indicate that, at minimum, another 10 Sv of northward flow are required to balance top-to-bottom mass (which is well constrained). This suggests that the Somali Current, although unmeasured at the western boundary on the 5 June (Beal and Chereskin, 2002), must be flowing through the section on average during its occupation. This makes sense in terms of both historical studies and contemporary satellite data, and is discussed in detail in Beal and Chereskin (2002). In order to reconcile the June circulation and obtain a mass balance, we therefore must assume that a mean Somali Current transport did exist to counter the large southward Ekman transport. However, estimating the exact size of the WBC is subject to large error. We attempted to constrain its size using estimates of Arabian Sea upwelling

flux made from wind and hydrographic data (Smith and Bottero, 1977), which indicated that 8 Sv of water upwell within the Arabian Sea through the 50 m level. Thus, we placed an upwelling flux of O(10) Sv from layer 3 into layers 1 and 2 in the inverse calculation, resulting in a Somali Current of 16 Sv for June. This approximation is flawed due to the aforementioned layer thickness changes.

Another concern over the June section is the noisy geostrophic shear in the east, where the cruise track was forced south over relatively shallow topography to avoid Indian waters. The noise is highly barotropic and causes transport fluctuations of the order of the overall basin transport; thus it may disguise the overall basin 'slope' in dynamic height. Owing to the difficulties with the June circulation, the resulting heat and salt transports are subject to large error.

In addition to its variability, the Arabian Sea exhibits a deeply ventilated water column. Ventilation to the north of 8°30′N reaches depths of over 1000 m, which means that salt (and heat) is not conserved above intermediate depth. Waters formed in the centre of the Arabian Sea during the southwest monsoon are exported at the surface, waters ventilated in the Persian Gulf flow across 8°30′N at thermocline depths (200–400 m), and waters ventilated in the Red Sea pour over the sill at Bab El Mandeb to spread at depths of between 500 and 1000 m. This reduces the number of constraints in the inverse problem considerably, leaving the upper layers constrained only by mass conservation. As a result we have used the air–sea volume fluxes of Weller et al. (1998) to better constrain the ventilated layers of the model. This is similar to the method of Sloyan and Rintoul (2001), except that no heat balance is implemented here and therefore we do not utilise air–sea heat fluxes.

4.2.2. Direct velocities and the geostrophic streamfunction

Before discussing aspects of the June and September circulations that result from our inverse model, it is helpful to look at the vertical velocity fields and note the important features and changes. These are shown in Fig. 6. In June the Great Whirl is yet to fully develop and appears as a small, surface trapped feature (Fig. 6, top panel) with a maximum velocity of about 60 cm s^{-1} which penetrates no deeper than 200 m. It is positioned right on the western boundary, possibly cutting off the northward flowing Somali Current temporarily. There is some intensification of northward flow at intermediate depth on the western boundary, and a southward DWBC is seen by both steeply sloping isopycnals and direct velocities (not shown, Beal et al., 2000a, b). A second, weaker, anticyclonic eddy sits on the eastern flank of the first and is also very shallow. Close to the eastern boundary, over the Chagos-Laccadives Ridge there is much mesoscale structure and weak, noisy velocities at depth. By September (Fig. 6, bottom panel) the Great Whirl is strong and deep and is positioned farther east, with a strong Somali Current flowing northward in-shore of it. Maximum velocities are 150 cm s^{-1} at the surface and over 10 cm s^{-1} at 3000 m depth, making the feature strongly barotropic. The dynamic structures of the Somali Current and Great Whirl fill the Somali Basin. On the eastern flank of the Whirl is a small, shallow eddy (200 m) and a third anticyclonic eddy sits at the eastern boundary. Elsewhere (in the interior) velocities are small with a barotropic nature, possibly as a result of the downward propagation of Rossby and Kelvin waves.

The horizontal circulation of water masses within each density layer is illustrated in Fig. 7, which shows the Sverdrup transport streamfunctions (from the inversion) for June and September. These cumulated transports show all elements of the circulation including the Ekman layer, the extrapolated Somali Current, and DWBC. A shallow Ekman layer is responsible for the large export of waters at the surface (above 50 m) in June. The southward Ekman transport accumulates linearly from east of 56°E out to 72°E, coincident with the Chagos-Laccadives Ridge. In September, waters are exported primarily from layer 2, owing to a deepened Ekman layer and to a large slope in dynamic height from east of the Great Whirl to about 68°E. The Great Whirl is present through layers 1 and 2 down to 200 m in June, with further anticyclonic circulation evident in the NIDW and CDW layers (5 and 6). In the

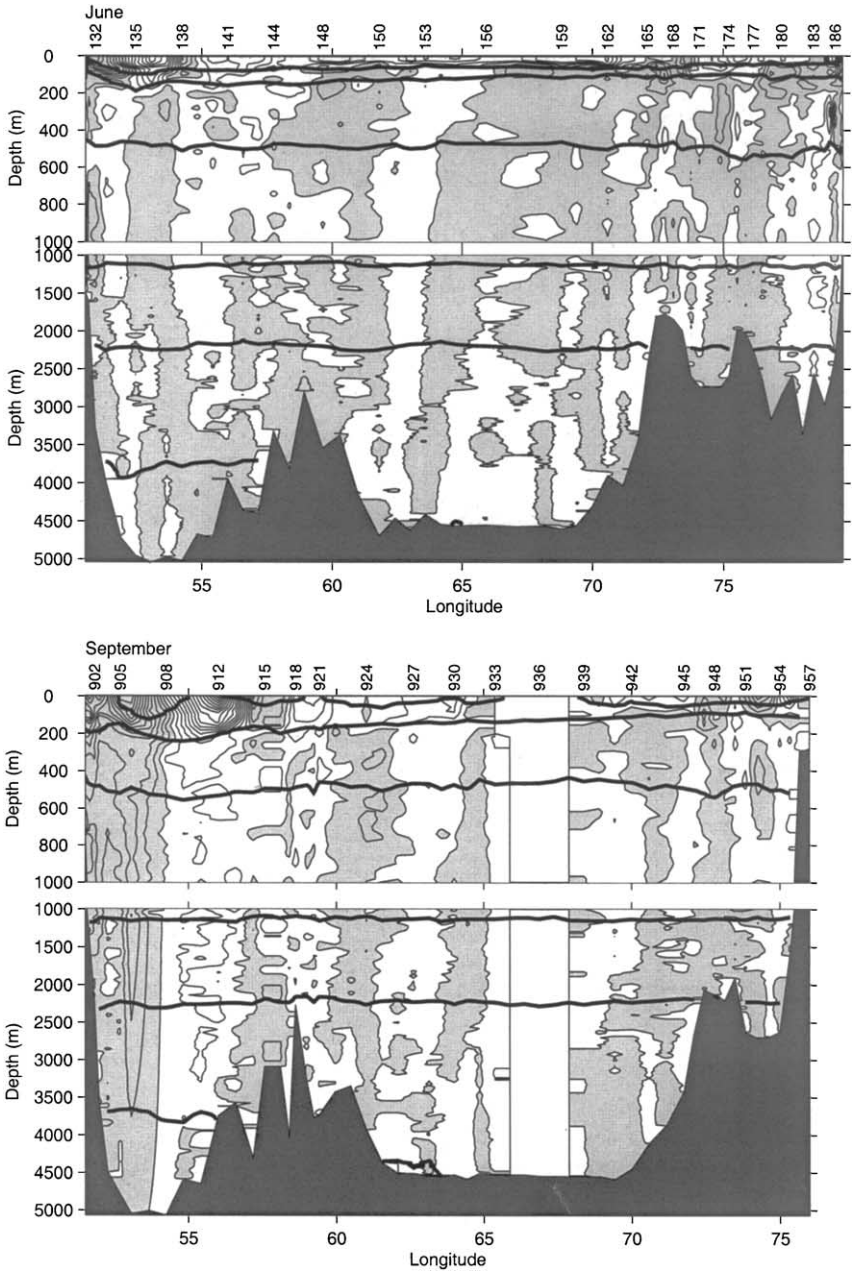

Fig. 6. Vertical section of LADCP velocities in (a) June, and (b) September. Depth is split at 1000 m to enhance the upper water column. Contours are every 10 cm s^{-1} northward velocities are shaded grey.

subsurface layers in June the accumulated transports are noisy, particularly at the eastern boundary, resulting in large uncertainties in the net layer transports. In the PGW, RSW and NIDW layers (3, 4 and 5), water masses that we expect to have an annual-mean export of waters, there is significant southward flow to the west and east of the Carlsberg Ridge in June and these southerly flows

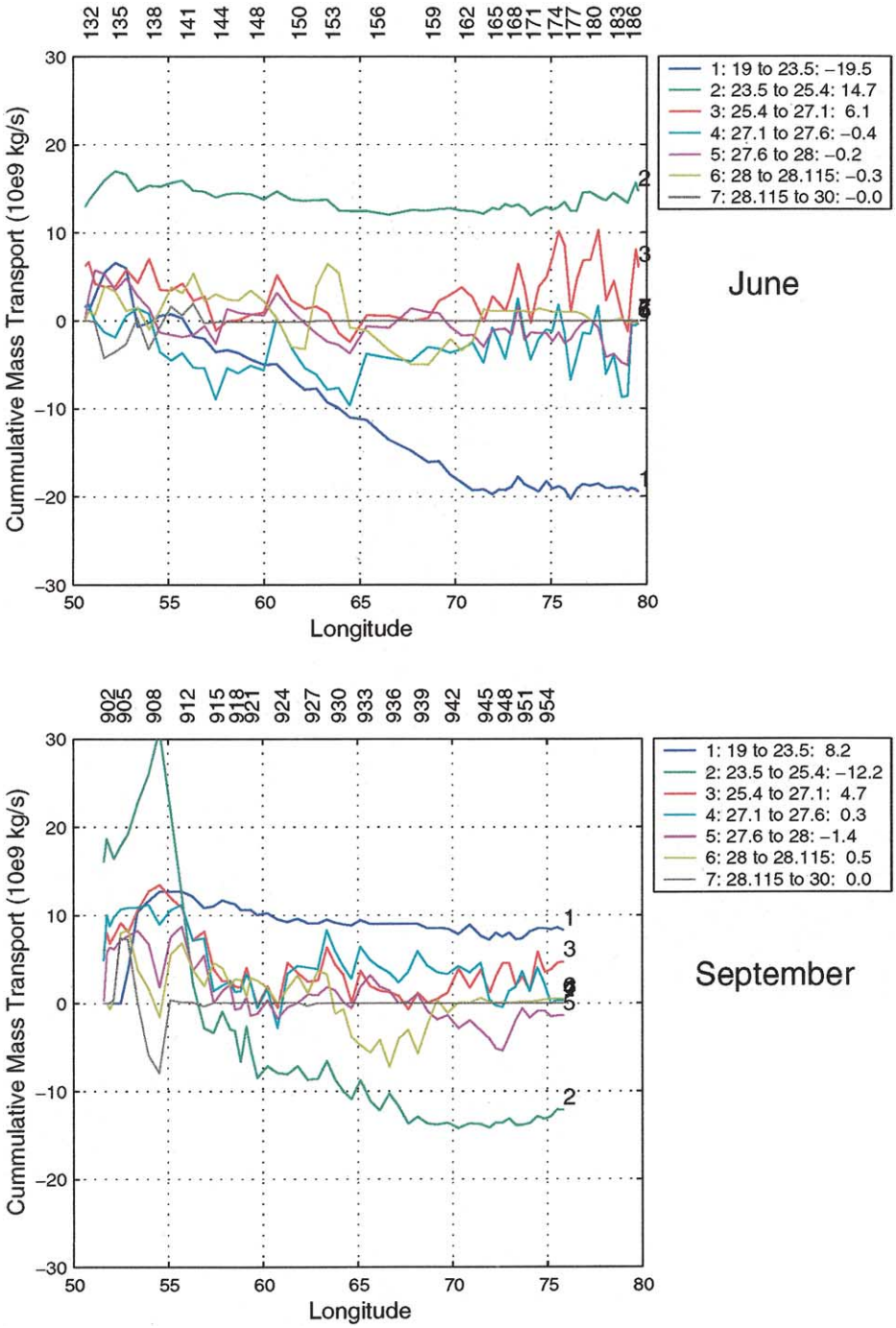

Fig. 7. Cumulative mass transport along 8°30′N in each water mass layer (see Table 1) for (a) June, and (b) September. Transport given in units of $10^9\,\mathrm{kg\,s^{-1}}$. Every third station labelled along top axis. Legend shows layer number, neutral density class, and cumulative mass transport.

coincide with higher salinities in the RSW layer, indicating more northerly waters that have been advected onto the section (Fig. 2a). In September the PGW, RSW and NIDW layers also show southward transport on the eastern flank of the Great Whirl and over the Carlsberg Ridge. Less significantly, there is a small southward flow over the Chagos-Laccadives Ridge (72°E) within the RSW layer. These flows are both coincident with the appearance of patches of warmer and saltier RSW over the ridges (Fig. 5) in September. As for the deep and bottom waters in September, there is a southward advection of CDW in the Arabian Basin in contrast to a generally northward advection in the Somali Basin. The bottom layer of dense CDW, which fills only the Somali Basin, has a cyclonic rotation, opposite to the Great Whirl in June, and a strong O (8 Sv) anticyclonic rotation in September.

4.2.3. Overturning

Fig. 8 shows the overturning geostrophic mass transport ($\bar{u}\bar{\rho}$) for June (blue) and September (red). The thin lines depict the circulation referenced to the neutral surface where $\gamma = 28$ (2200 m), and balanced for zero mass divergence using a single uniform velocity correction across the section, after Bryden et al. (1991). The thick lines show the inverse results. Only the geostrophic transports are shown: for June this does not include the 16 Sv Somali Current (which cannot be extrapolated using hydrographic measurements), nor the 3 Sv DWBC, nor the −19.7 Sv Ekman transport, although these transports were present in the inverse equations; for September this does not include the −7.3 Sv Ekman transport, but does include the Somali Current, for which an onshore extrapolation was constructed based on transport from underway ADCP (Beal and Chereskin,

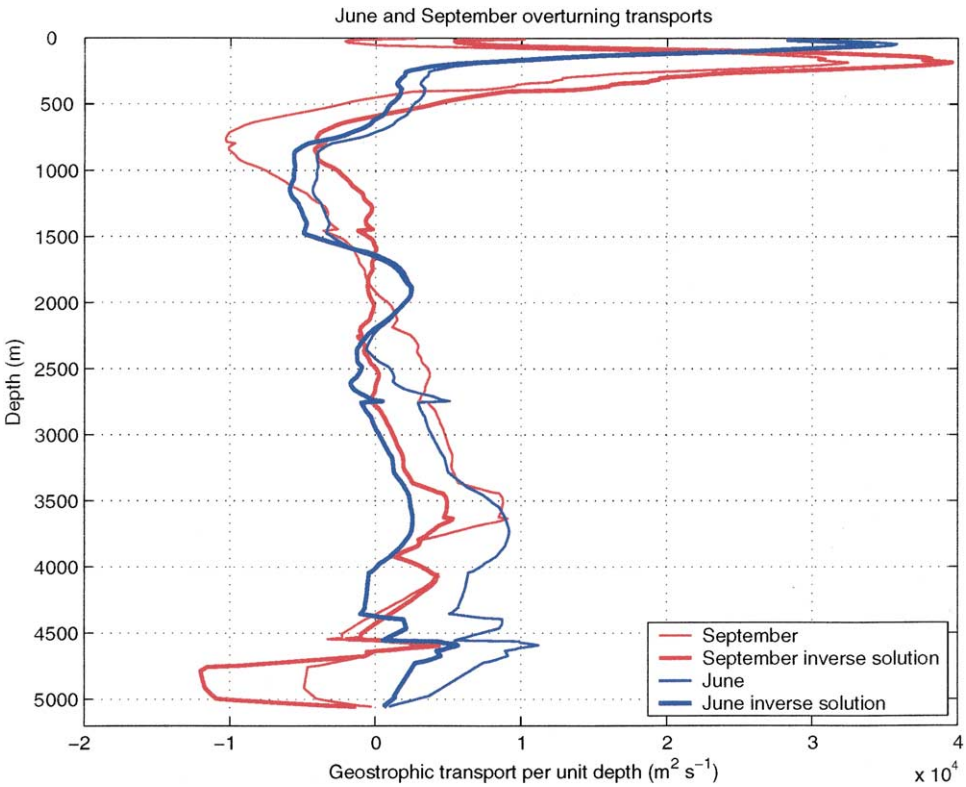

Fig. 8. Overturning mass transports (averaged along depth surfaces) for June (blue) and September (red). Thin lines show the simple solution, thick lines show the inverse solution (see text for explanation).

2002). This figure is provided as a useful comparison to other papers that present simple geostrophic overturning transports.

There appear to be two main overturning cells in both June and September. A strong shallow cell where water is exported within the Ekman layer and replaced by waters from immediately below (O(10 Sv)), and a far weaker cell where deep waters flow into the basin from the south and upwell to leave at intermediate depth (O(1 Sv)). The shallow cell is closed above about 500 m on both occupations. The inverse calculation acts to reduce the deep overturning cell considerably compared to the simple circulation. This results from both the salt and silica conservation and because the magnitude of vertical velocities (w^*) in the deep ocean are unrealistically large for the simple circulation. The differences between the June and September circulations largely result from the deepening and strengthening of the Somali Current from June to September, the strengthened interior geostrophic transport in September, and from the reversal of the DWBC from northward in June to southward in September. Although the latter has not been shown in detail in this manuscript, the reversing DBWCs were examined by Beal et al. (2000a, b). It is not useful to examine the bottom waters in Fig. 7 in terms of vertical overturning, since the isopycnals below 3800 m slope considerably, with far denser water filling the Somali Basin than the Arabian Basin, due to the ridge topography. For an examination of dianeutral overturning transports (in terms of water masses), the top panels of Fig. 9a and b, show the net transports of our model neutral density layers 1–7, as described in Table 1.

In Fig. 9 all transport components are represented (if not explicitly): Ekman (pink), Somali Current and DWBC (red), and the net circulation (blue), which is made up of the sum of the other two components, plus the interior component (from the inverse), which is not shown independently. In June the upper overturning cell is very strong, with 5.4 Sv of upwelling required from the thermocline (layer 3) to balance the large Ekman transport in the surface layers. (Recall that layers 1 and 2 are treated as one in the model because both outcrop within the Arabian Sea). This is an average upwelling velocity of 1.4×10^{-4} cm through approximately the 150 m level. However, recall that the Levitus climatology shows that layer 3, the thermocline, is thinning throughout the Arabian Sea in June, July and August (while the upper layers are thickening). If storage effects were to balance the mass convergence we see in the circulation in layer 3 (Fig. 9) and negate upwelling, we would expect a thickening of the layer. Instead, the layer is losing mass, implying an additional upwelling of O(10 Sv) over and above that diagnosed by the inverse model. This results in a total upwelling closer to 15 Sv (4.2×10^{-4} cm s^{-1}) through the TTP. Most of the upwelled waters are replaced by the Somali Current, which flows into the Arabian Sea at a cooler temperature and higher density than the subtropical surface waters of the Ekman layer. Below 500 m there is an overall weak export of all intermediate and deep water masses. The geostrophic transport is so weak in June that the circulation is completely dominated by the Ekman layer. However, Fig. 8 shows that there is some structure at depth, with export above 1700 m (eroded by Somali Current transport in the inverse solution) and generally an import of waters below. In layer 7, which represents the bottom waters of the Somali Basin, the 3 Sv DWBC is balanced by a northward geostrophic flow in the interior at the same density and thus there is no significant upwelling through the top of this layer. This is largely as a result of the interface occupying a very small area north of 8°30′N.

In September the Ekman transport has deepened and now most of it lies at the same density (layer 2) as the maximum Somali Current transport. In contrast to June, the geostrophic transport component is now significant throughout the water column, acting to balance the Somali Current input. There is a substantial net influx of mass into layer 3, as there was in June, but this time the Levitus climatology indicates that this layer (the pycnocline) is thickening in September (as the winds weaken), so that storage easily compensates the convergence of mass and there is no significant upwelling to the north of our line. Thus, the shallow overturning cell of June is essentially 'switched off' by September. The

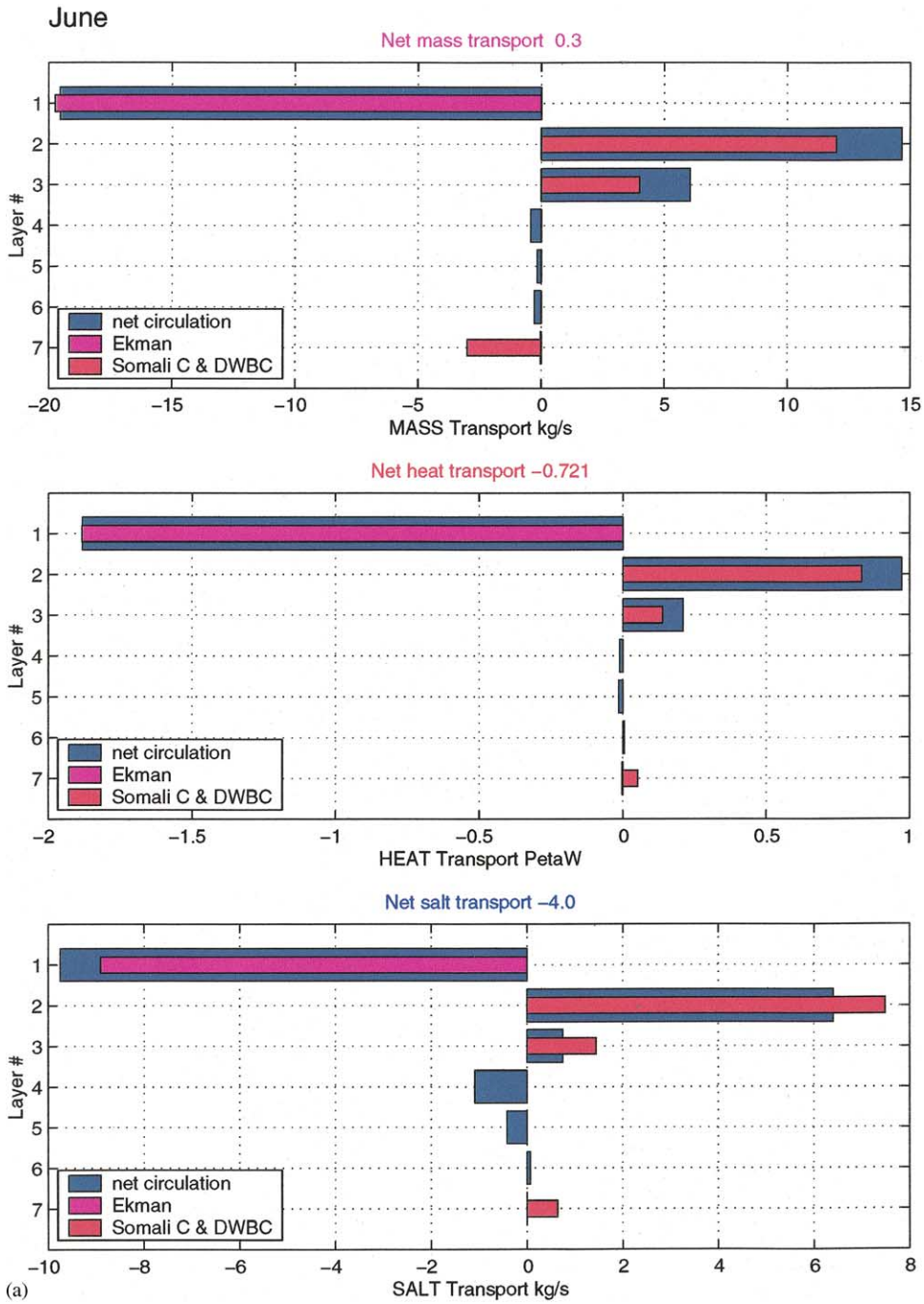

Fig. 9. Net layer transports of mass (top panel), temperature (middle panel) and salt (bottom panel) across 8°30′N in (a) June, and (b) September. Thick blue bars show the net circulation, pink bars show the Ekman component, and red bars show the Somali Current and Deep WBC components. For the net circulation there is an additional interior component of transport (see Table 2).

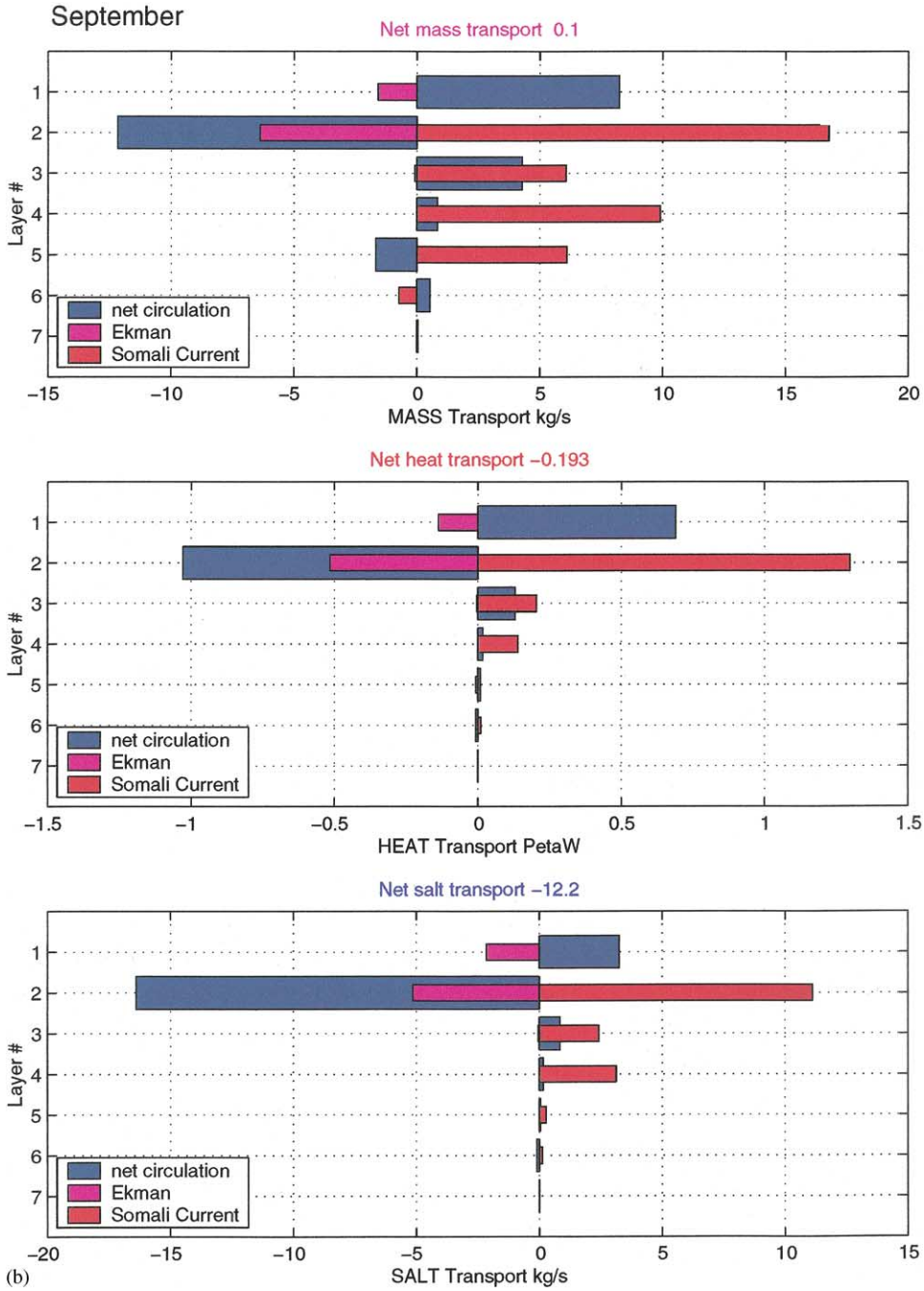

Fig. 9 (*continued*).

balance of mass in the upper layers is now dominated by a horizontal exchange of interior geostrophic transport versus the Somali Current at the boundary, in contrast to June where the Ekman component dominates, causing a strong vertical exchange. The deep overturning cell is

small, with an export of 1.7 Sv of NIDW from layer 5, and a weak influx of CDW below. There is an export of RSW from the interior in September, but at the boundary the deepened Somali Current overwhelms the interior southward flow and the net transport of RSW is northward. This pattern of RSW transport ties in with the findings of Beal et al. (2000a, b), who saw that there was less RSW present at the western boundary of the Arabian Sea during the southwest monsoon. We speculate that the export of RSW at the western boundary is only stemmed during the late summer monsoon when the Somali Current runs deep. There is 0.8 Sv of upwelling through the $\gamma = 28$ surface (2200 m level), representing an upwelling velocity of $3.2 \times 10^{-5}\,\mathrm{cm\,s^{-1}}$. This agrees closely with the overall Indian Ocean upwelling estimate by Robbins and Toole (1997), who used hydrographic data at 32°S to construct an inverse calculation.

4.2.4. Heat and salt fluxes

The net mass, heat and salt transports for both June and September are split into the vertical (or mean layer, $\bar{u}\bar{C}$) transports and the horizontal (or eddy layer, $u'C'$) transports (after Bryden et al., 1991) and shown in Table 2 (Fig. 9 illustrates the net heat and salt transports in each water mass layer). The transports are calculated with reference to mean reservoir values of temperature and salinity (and thus are effective heat and salt transports, rather than temperature and salinity transports relative to an arbitrary scale). We chose the reservoir values as the average of the two section-means, 5.5631°C and 34.938 psu, so that they are the same values for both June and September, making each transport directly comparable.

Looking at the net transports in Table 2 and Fig. 9 it is clear that the dominant balance has changed from June to September. In June the mass, heat and salt balances are dominated by the Ekman component and the Somali Current, while in September the balance is predominantly between the geostrophic interior transport and the Somali Current. In June the Ekman layer exports −1.88 PW of heat from the Arabian Sea, more than can be counterbalanced by the WBC (1.03 PW) and by the smaller components of interior geostrophic flux (0.14 PW) and net solar radiation (0.36 PW). The latter value is taken from

Table 2
Net, vertical, and horizontal (eddy) transports of mass, heat, and salt across 8°30′N in the Arabian Sea in June and September 1995. Transports are split into Interior, Ekman, and Somali (western boundary) components, with the Balance representing the sum of all three components

Property	June				September			
	Interior	Ekman	Somali	Balance	Interior	Ekman	Somali	Balance
		Net transport				Net transport		
Mass	7.00	−19.70	13.00	0.3	−29.99	−8.04	38.11	0.086
Heat	0.14	−1.88	1.03	−0.72	−1.18	−0.66	1.65	−0.19
Salt	−4.60	−8.93	9.57	−3.96	−21.79	−7.32	17.15	−12.16
		Horizontal component				Horizontal component		
Mass	0	0	0	0	0	0	0	0
Heat	−0.068	−0.056	0.048	−0.076	−0.170	−0.029	0.066	−0.132
Salt	−6.51	1.06	−0.32	−5.766	−7.13	0.43	−3.62	−10.32
		Vertical component				Vertical component		
Mass	7.00	−19.70	13.00	0.3	−29.99	−8.04	38.11	0.086
Heat	0.20	−1.82	0.98	−0.64	−1.01	0.63	1.58	−0.06
Salt	1.91	−9.99	9.89	1.81	−14.66	−7.74	20.77	−1.84

Units: Mass: $10^9\,\mathrm{kg\,s^{-1}}$, Heat: PW, Salt: $10^6\,\mathrm{kg\,s^{-1}}$. Heat transports are given relative to the sections-mean potential temperature 5.5631°C. Salt transports are given relative to the sections-mean salinity 34.938. Somali component in June includes the Deep Western Boundary Current.

the SOC climatology of Josey et al. (1996) and is for all waters to the north of 8°30′N over the month of June 1995. As a result, the Arabian Sea is cooling at a rate of −0.36 PW in June (the net heat transport balance from Table 2 plus net solar radiation). Ninety per cent of this cooling results from the vertical transport component (Table 2), which represents the shallow overturning cell discussed above. This cell is driven by Ekman divergence, which forces upwelling of subsurface waters near the coasts to the north. Little of the heat divergence results from eddy fluxes.

By September the Somali Current has strengthened into the major transport component, importing 1.65 PW of heat at the western boundary. The interior geostrophic transport is now southwards and exports −1.18 PW of heat, mainly as ASSW (layer 2). The weakened Ekman layer transport is −0.66 PW and the net solar radiation, estimated for the month of September 1995 from the SOC climatology, is 0.32 PW. Thus, the heat budget is almost closed, with only a small implied storage of 0.12 PW. This time 70% of the oceanic heat flux divergence results from horizontal or eddy fluxes, representing an exchange of water masses by the gyre circulation. This is a reflection of the change of predominant mass balance in the system, which is owing to the tilting of isopycnals to produce an interior geostrophic flux. We hypothesise that in June the gyre circulation is yet to 'spin up' in response to the southwest monsoon winds: there is no cross-basin pressure gradient. By September, the circulation more closely resembles other, steady subtropical gyres of the world's oceans, with an equatorward geostrophic interior transport closed by poleward flow within a WBC.

The net exchange of salt across 8°30′N does not follow the pattern of heat transport. In June there is a small export of salt ($-3.96\times10^6\,\mathrm{kg\,s^{-1}}$), which is entirely carried by the interior, horizontal circulation. It results from an inflow of BBW at the surface in the east (a remnant current from the intermonsoon circulation), the Ekman layer, and from an outflow of RSW at intermediate depths (Fig. 9a, bottom panel). In September there is also a net export of salt ($-12.16\times10^6\,\mathrm{kg\,s^{-1}}$), which results almost exclusively from the production and southward advection of ASSW within the Ekman layer. Where we expect a removal of salt via the RSW and NIDW layers on average, at this time of year any southward flow in the interior has been overwhelmed by the strong, deep, late-monsoon Somali Current.

In order to estimate a freshwater flux across 8°30′N it is usual to assume that measured salinity and geostrophic velocity fields are in a steady state (e.g., Wijffels et al., 2001). Then we would take the salt divergences in Table 2 and imply an E-P flux, assuming that the salt transport compensates the freshwater exchange through the ocean surface. However, in the case of the Arabian Sea we have seen that the monsoon variability causes large seasonal changes in the surface and intermediate salinity field and in the flow field. Thus, there is a seasonal storage of salt north of 8°30′N, and as a result a compensatory salt flux of order $-10\times10^6\,\mathrm{kg\,s^{-1}}$ is implied across 8°30′N during the summer monsoon (Stramma et al., 2002). This flux is the same order of magnitude as the net salt fluxes derived from the inverse model for June and September (see Table 2) and thus only a minor part of the salt divergence acts to compensate the E-P balance. Therefore, because we could not reliably diagnose the freshwater flux from the oceanic data, we decided to include estimated E-P fluxes from Weller et al. (1998), as described in Section 3 above, as additional (loose) constraints in the inverse models.

5. Discussion and conclusions

It has been suggested previously (e.g., Stramma et al., 2002—hereafter Stramma) that the temporal change in water properties along a zonal line close to 8°30′N is due to the heaving of isopycnals by Rossby waves. Rossby waves are a large source of variability in the Arabian Sea, and our analysis of TOPEX/Poseidon SSH anomalies at 8°30′N shows that it is forced annual waves of wavelength 3150 km and amplitude 400 mm that are dominant. According to their speed, they are second baroclinic mode waves, so that the density differences they cause in the central Arabian Sea reverse sign in the deep ocean (Brandt et al., 2002).

However, although the cross-basin isopycnal structure is certainly effected by the Rossby waves, we find that on the average the change in water mass structure along 8°30′N is not as one might predict based on SSHA. Fig. 10 shows the temporal change in SSHA averaged along 8°30′N, from 1995 to 1999. The amplitude of the mean signal along the 8°30′N section is just one-quarter the Rossby wave amplitude, because the Rossby wavelength is just a little greater than the basin width and thus, when the sea surface is raised in the west, it is lowered in the east and vice versa. The zonal mean SSHA is therefore a residual, representing the seasonal variability at 8°30′N. The southwest monsoon season of 1997 is clearly anomalous, owing to the strong El Nino of 1997/98.

Looking specifically to the times of our occupations in 1995 (crosses in Fig. 10), the mean SSH (from TOPEX/Poseidon) is 50 mm less along the section in September than in June. Over the whole basin area it is 70 mm less, as discussed previously. Following the two-layer-ocean argument of Chambers et al. (1997), this would imply an integrated loss of heat content from the water column. This is because, in a two-layer ocean, a raising of the thermocline (cooling) is expected in response to a lowering of SSH. However, the water properties along the section (Fig. 3) are overall warmer and saltier in September than in June in both the west and the east and wind mixing has caused a lowering of the TTP, rather than the expected raising. Therefore, dynamic height is actually greater in September than in June (circles in Fig. 10), while SSHA is less. Moreover, the large property changes along neutral surfaces (Fig. 5) lead us to conclude unequivocably that the vertical displacement of density surfaces by Rossby waves is not the dominant cause of changes in heat and salt content along 8°30′N over the course of the southwest monsoon. A passing Rossby wave would vertically displace a neutral surface, but not change the water mass properties along that surface. Instead, the property changes must result from an advection of warmer, saltier waters onto the section, except at the surface where the changes are driven by air–sea interaction. Clearly then, care should be taken when interpreting large-scale SSHA changes in the Arabian Sea to signify oceanic heat content (Manghnani et al., 2002), because the barotropic component of sea-level change—in this case the loss of mass from the basin during the southwest monsoon—may be comparable to the heat storage component.

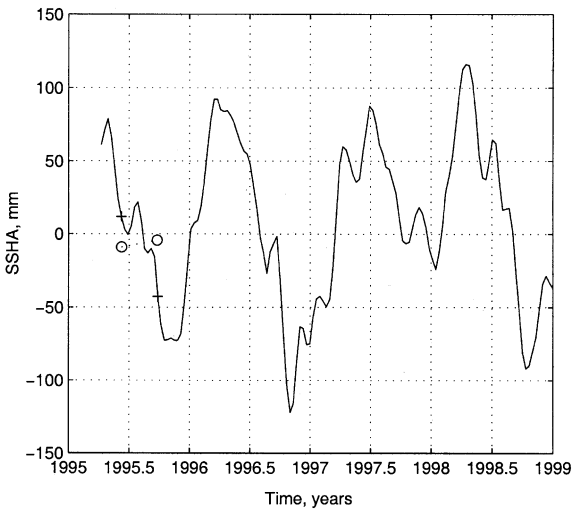

Fig. 10. Temporal variation of Sea-Surface Height Anomaly (SSHA) averaged along 8°30′N in the Arabian Sea. SSHA is from TOPEX/Poseidon and has been smoothed by a running 30-day mean. Plus symbols depict the times of the June and September cruises. Circles show the in-situ SSHA from June and September. This was calculated using section dynamic height, plus a correction from the inverse solution, minus the climatological dynamic height from Levitus 94 data. Dynamic heights were integrated from 2000 dbar, and therefore we have assumed that the pressure field does not vary below this.

So, the warm, salty water along 8°30′N must originate in the Arabian Sea, but from how far north does it come? WOCE line I7 is a quasi-meridional section that crossed perpendicular to 8°30′N at 64°E in August 1995, then turned northwestward at 15°N, towards the coast of Oman. Therefore, the section provides a meridional water mass field contemporary to our data. Temperature and salinity sections along I7 down to mid-depth are shown in Fig. 11. The waters get warmer and saltier to the north along neutral surfaces, except above the 18°C isotherm, where cooling and freshening are controlled by wind mixing, evaporation and upwelling. On the 8°30′N

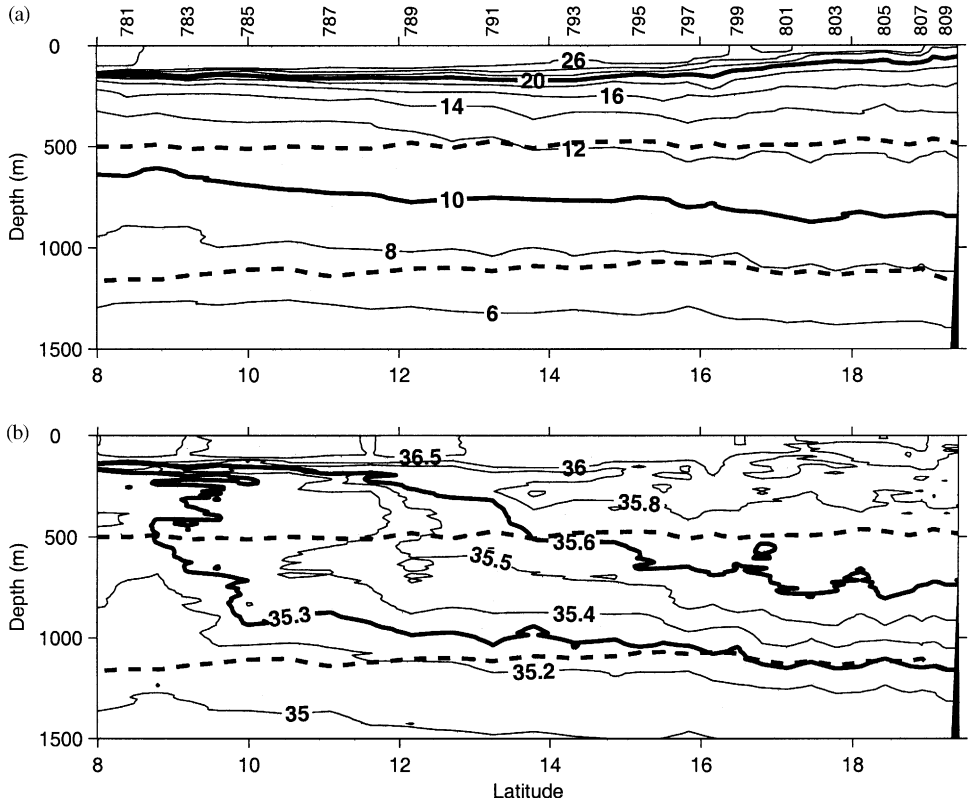

Fig. 11. Vertical sections of (a) potential temperature, and (b) salinity down to mid-depth, along quasi-meridional WOCE line I7. Dashed lines are neutral surfaces at 27.1 and 27.6, which demark the Red Sea Water layer.

section, along the upper interface of the RSW layer ($\gamma = 27.1$) salinity increases by 0.06 from June to September (Fig. 4). The meridional gradient of salinity along this neutral surface from the I7 data is approximately 0.3 over 500 km (Fig. 11). Therefore, waters advected from about 100 km to the north could cause the 0.06 salinity change at 8°30′N. This seems reasonable, resulting in a mean southward advection rate of about 1 cm s^{-1} during the southwest monsoon (there are 100 days between the June and September occupations). It is possible that meridional advection could result from Rossby waves, but we speculate that the general southward migration of the water column (above 1500 m), combined with the drop in sea level throughout the basin, indicates a removal of mass from the Arabian Sea over the course of the southwest monsoon. Effectively, the monsoons cause a seasonal 'sloshing' of water into (northeast monsoon) and out of (southwest monsoon) the Arabian Sea.

We find two distinct overturning cells in both June and September. The shallow cell has a magnitude of approximately 15 Sv in June and 0 Sv in September, being highly variable in strength and direction on a seasonal basis, we expect it to stem in the intermonsoon period and reverse completely during the northeast monsoon. During the southwest monsoon this cell is driven by Ekman divergence of surface waters, and by water mass formation processes (evaporation and mixing) which erode the thermocline and thicken the surface layer. Our estimates of upwelling to the surface are much larger than the numbers of (Shi et al. (2000)), who estimate an average 1.4 Sv of upwelling, but in the Omani region alone, and larger than the 8 Sv suggested by Smith and Bottero (1977).

The second, deep overturning cell is weak and is diagnosed poorly in June, but in September it is associated with 0.8 Sv of upwelling through the 2200 m level. This is very much less than values from Stramma and Shi et al. (2002, hereafter Shi), who estimated 4–6 and 7 Sv, respectively. The difference results from two factors: Neither Shi nor Stramma have an accurate treatment of the WBC, nor do they consider realistic, large-scale oceanic upwelling velocities. For the WBC, Stramma were constrained by lack of measurements to estimate fluxes while avoiding the western boundary, and Shi restricted themselves to the use of geostrophic velocities when estimating the transport of the Somali Current, which we undertook in some detail utilising direct measurements (Beal and Chereskin, 2002). As far as upwelling velocities are concerned, our inverse model imposes a constraint on w^* to be of order $5\times10^{-5}\,\mathrm{cm\,s^{-1}}$ in the deep ocean. This is generous at two and a half times the generally accepted basin-averaged vertical velocity of the Pacific and one and a half times the Indian Ocean value given by Robbins and Toole (1997). Taking the deep overturning magnitudes of Stramma and Shi as order 5 Sv, we can estimate their resulting average vertical velocity for the Arabian Sea. At 2200 m (bottom of NIDW layer) the area of the Arabian Sea is $2.75\times10^{12}\,\mathrm{m^2}$, according to the Smith and Sandwell (1997) topographic database. This gives a w^* of $1.8\times10^{-4}\,\mathrm{cm\,s^{-1}}$, that is 5 times the Indian Ocean average from Robbins and Toole (1997). Such a large average upwelling as this seems physically unlikely, since although w^* is likely enhanced by the rough topography of the Carlsberg and Chagos-Laccadives Ridges, the majority of the basin's seabed consists of a smooth alluvial fan (Fig. 1). Thus, we prefer our deep overturning estimate of order 1 Sv for the Arabian Sea.

Our estimates for the total heat transport across 8°30′N are −0.72 PW in June and −0.19 PW in September. The September heat divergence is small compared to both other recent direct estimates and this is mainly as a result of the size of our Somali Current, which acts to replace much of the heat lost via the Ekman layer. Stramma estimates a heat transport of −0.62 PW in August and Shi estimates −0.6 PW. Shi uses the same WOCE data as we use in September, but without the direct measurements, which reveal large bottom velocities in the WBC. Shi claim that as much as −0.28 PW is exported below 2000 m, whereas we find the heat divergence in our layers 6 and 7 (below 2200 m) to be negligible. Their large heat transport results principally from a large deep mass transport, which we consider unlikely (see above). In our circulation it is the surface circulation that dominates the heat flux and the large northward Somali Current component drives heat export down in September. For our analysis, the WBC volume transport was diagnosed (Beal and Chereskin, 2002), by extrapolating the geostrophic velocity field using direct velocities, which approach the Somali Coast to within waters of less than 200 m depth. The resulting Somali Current estimate is 38 Sv and carries a heat transport of 1.65 PW, dominating the heat balance in that month. The Somali Current is extremely variable at 8°30′N, as studies of satellite altimetry and regional models have shown (Wirth et al., 2002), and this variability may account for the difference between our transport and that of Stramma a month earlier (the Ekman transports are similar). We expect the basin heat transport to pass through zero later during the intermonsoon period, since the dominant component, the Ekman transport, changes sign to flow northward during the northeast monsoon.

Although our fluxes are approximate due to the variability of the circulation in the Arabian Sea (we have not quantified errors using the inverse residuals because we do not think they are meaningful in light of the variability) we think the diagnosis of separate shallow and deep overturning cells is robust. Moreover, we find the changing of the dominant balances from June to September insightful. A non-geostrophic exchange of Ekman divergence versus the Somali Current drives a strong upwelling (and loss of mass from the thermocline) in June, and a more familiar horizontal exchange of the geostrophic interior versus the WBC dominates in September.

Acknowledgements

The June and September transects across the Arabian Sea at 8°30′N were supported by the

National Oceanic and Atmospheric Administration and the National Science Foundation, respectively. We acknowledge Bob Molinari as the Chief Scientist on the RV *Baldridge*. Thanks to all the scientists and crew aboard the *Baldridge* and the *Knorr* for their hard work at sea. Lisa Beal would especially like to thank Paul Robbins for his advice and sharing of software. We used SSH anomalies as generated by the AVISO group, from TOPEX/POSEIDON and ERS satellite altimetry observations (http://www-aviso.cls.cnes.fr). We thank an anonymous reviewer for insightful comments on storage, which led to an improvement of the manuscript. We acknowledge support from NSF Grant OCE99-06776.

References

Beal, L.M., Chereskin, T.K., 2002. The volume transport of the Somali Current during the 1995 southwest monsoon. Deep-Sea Research II, this issue.

Beal, L.M., Molinari, R.L., Chereskin, T.K., Robbins, P.E., 2000a. Reversing bottom circulation in the Somali Basin. Geophysical Research Letters 27, 2565–2568.

Beal, L.M., Ffield, A., Gordon, A.L., 2000b. Spreading of Red Sea overflow waters. Journal of Geophysical Research 105, 8549–8564.

Brandt, P., Stramma, L., Schott, F., Fischer, J., Dengler, M., Quadfasel, D., 2002. Annual Rossby waves in the Arabian Sea from TOPEX/POSEIDON altimeter and in-situ data. Deep-Sea Research II 49, 1197–1210.

Bryden, H.L., Beal, L.M., 2000. Role of the Agulhas current in Indian Ocean circulation and associated heat and freshwater fluxes. Deep-Sea Research I 48, 1821–1845.

Bryden, H.L., Roemmich, D.H., Church, J., 1991. Ocean heat transport across 24°N in the Pacific. Deep-Sea Research 38, 297–324.

Chambers, D.P., Tapley, B.D., Stewart, R.H., 1997. Long period ocean heat storage rates and basin-scale heat fluxes from TOPEX. Journal of Geophysical Research 102, 10525–10533.

Chapman, P., Mostert, S.A., 1990. Does freezing of nutrient samples cause analytical errors? South African Journal of Marine Science 9, 239–247.

Chereskin, T.K., Wilson, W.D., Bryden, H.L., Ffield, A., Morrison, J., 1997. Observations of the Ekman balance at 8°30′ in the Arabian Sea during the 1995 southwest monsoon. Geophysical Research Letters 24, 2541–2544.

Chereskin, T.K., Wilson, W.D., Beal, L.M., 2002. The Ekman temperature and salt fluxes at 8°30′N in the Arabian Sea during the 1995 southwest monsoon. Deep-Sea Research II 49, 1211–1230.

Düing, W., Leetmaa, A., 1980. Arabian Sea cooling: a preliminary budget. Journal of Physical Oceanography 10, 307–312.

Egbert, G.D., Bennett, A.F., Foreman, M.G.G., 1994. TOPEX/POSEIDON tides estimated using a global inverse model. Journal of Geophysical Research 99, 24821–24852.

Fieux, M., Stommel, H., 1977. Onset of the southwest monsoon over the Arabian Sea from marine reports of surface winds—structure and variability. Monthly Weather Review 105, 231–236.

Fischer, A.S., Weller, R.A., Rudnick, D.L., Ericksen, C.C., Lee, C.M., Brink, K.H., Fox, C.A., Leben, R.R., 2002. Mesoscale eddies, coastal upwelling and the upper ocean heat budget in the arabian sea. Deep-Sea Research II 49 (12), 2231–2264.

Flatau, M.K., Flatau, P.J., Rudnick, D., 2001. The dynamics of double monsoon onsets. Journal of Climate 14, 4130–4146.

Fleurant, C.I., Molinari, R.L., 1998. Comparison of bottle salinity and bottle oxygen values from WHP repeat lines I7N, I1W, I8N and I8S. International WOCE Newsletter 33, 27–29.

Gamsakhurdiya, G.R., Meschanov, S.L., Shapiro, G.K., 1991. Seasonal variations in the distribution of Red Sea waters in the northwestern Indian Ocean. Oceanology 31, 32–37.

Ganachaud, A., Wunsch, C., Marotzke, J., Toole, J., 2000. The Meridional overturning of the large scale circulation of the Indian Ocean. Journal of Geophysical Research 105, 26117–26134.

Hastenrath, S., Greischar, L., 1993. The monsoonal heat budget of the hydrosphere-atmosphere system in the Indian Ocean sector. Journal of Geophysical Research 98, 6869–6881.

Hastenrath, S., Lamb, P., 1980. On the heat budget of hydrosphere and atmosphere in the Indian Ocean. Journal of Physical Oceanography 10, 694–708.

Jackett, D.R., McDougall, T.J., 1997. A neutral density variable for the world's oceans. Journal of Physical Oceanography 27, 237–263.

Josey, S.A., Kent, E.C., Oakley, D., Taylor, P.K., 1996. A new global air–sea heat and momentum flux climatology. International WOCE Newsletter 24, 3–5.

Levitus, S., Boyer, T.P., 1994. World Ocean Atlas 1994 Vol. 4: Temperature. NOAA Atlas NESDIS 4, US Department of Commerce, Washington, DC, 117pp.

Levitus, S., Burgett, R., Boyer, T.P., 1994. World Ocean Atlas 1994 Vol. 4: Salinity. NOAA Atlas NESDIS 3, US Department of Commerce, Washington, DC, 99pp.

Manghnani, V., Morrison, J.M., Xie, L., Subrahmanyam, B., 2002. Heat transports in the Indian Ocean using TOPEX/POSEIDON altimetry and model simulations. Deep-Sea Research II 49, 1459–1480.

Munk, W., Wunsch, C., 1998. Abyssal recipes II: energetics of tidal and wind mixing. Deep-Sea Research I 45, 1977–2010.

Oberhuber, J.M., 1988. An atlas based on the COADS data set; the budgets of heat, buoyancy, and turbulent kinetic energy at the surface of the global ocean. Max-Plank-Institute for Meteorology Report No. 15, 20pp, 247 Figs.

Polzin, K.L., Toole, J.M., Ledwell, J.R., Schmitt, R.W., 1997. Spatial variability of turbulent mixing in the abyssal ocean. Science 276, 93–96.

Robbins, P.E., Toole, J.M., 1997. The dissolved silica budget as a constraint on the meridional overturning circulation in the Indian Ocean. Deep-Sea Research I 44, 879–906.

Shi, W., Morrison, J.M., Bohm, E., Manghnani, V., 2000. The Oman Upwelling zone during 1993, 1994 and 1995. Deep-Sea Research I 47, 1227–1247.

Shi, W., Morrison, J.M., Bryden, H.L., 2002. Water, heat and salt flux at 8.5°N in the northern Indian Ocean. Deep-Sea Research II 49, 1231–1252.

Sloyan, B.M., Rintoul, S.R., 2001. The Southern Ocean limb of the global deep overturning circulation. Journal of Physical Oceanography 31, 143–173.

Smith, R.L., Bottero, J.S., 1977. On the upwelling in the Arabian Sea. In: Angel, M. (Ed.), A Voyage of Discovery. Pergamon Press, Oxford, pp. 291–304.

Smith, W.H.F., Sandwell, D.T., 1997. Global sea floor topography from satellite altimetry and ship depth soundings. Science 277, 1956–1962.

Stramma, L., Brandt, P., Schott, F., Quadfasel, D., Fischer, J., 2002. Winter and summer monsoon water mass and heat transport changes in the Arabian Sea near. Deep-Sea Research II 49, 1173–1196.

Swallow, J.C., Bruce, J.G., 1966. Current measurements off the Somali coast during the southwest monsoon of 1964. Deep-Sea Research 13, 861–888.

Weller, R.A., Baumgartner, M.F., Josey, S.A., Fischer, A.S., Kindle, J.C., 1998. Atmospheric forcing in the Arabian Sea during 1994–1995: observations and comparisons with climatology and models. Deep-Sea Research II 45, 1961–1999.

Wijffels, S.E., Toole, J.M., Davis, R., 2001. Revisiting the South Pacific sub-tropical circulation: a synthesis of world ocean circulation experiment observations along degrees S. Journal of Geophysical Research 106, 19481–19513.

Wirth, A., Willebrand, J., Schott, F., 2002. Variability of the Great Whirl from observations and models. Deep-Sea Research II 49, 1279–1295.

Wunsch, C., 1996. The Ocean Circulation Inverse Problem, Cambridge University Press, Cambridge, p. 442.